Editors' Suggestion

Tunable inter-moiré physics in consecutively twisted trilayer graphene

Wei Ren [1], Konstantin Davydov [1], Ziyan Zhu [2], Jaden Ma [3], Kenji Watanabe [4], Takashi Taniguchi,[5] Efthimios Kaxiras [6,7], Mitchell Luskin [8] and Ke Wang [1,*]

[1]*School of Physics and Astronomy, University of Minnesota, Minneapolis, Minnesota 55455, USA*

[2]*Stanford Institute for Materials and Energy Sciences, SLAC National Accelerator Laboratory, Menlo Park, California 94025, USA*

[3]*Department of Physics, The Ohio State University, Columbus, Ohio 43210, USA*

[4]*Research Center for Electronic and Optical Materials, National Institute for Materials Science, 1-1 Namiki, Tsukuba 305-0044, Japan*

[5]*Research Center for Materials Nanoarchitectonics, National Institute for Materials Science, 1-1 Namiki, Tsukuba 305-0044, Japan*

[6]*Department of Physics, Harvard University, Cambridge, Massachusetts 02138, USA*

[7]*John A. Paulson School of Engineering and Applied Sciences, Harvard University, Cambridge, Massachusetts 02138, USA*

[8]*School of Mathematics, University of Minnesota, Minneapolis, Minnesota 55455, USA*

(Received 16 November 2023; accepted 25 July 2024; published 3 September 2024)

We fabricated a twisted trilayer graphene device with consecutive twist angles of 1.33 ° and 1.64 °, in which we electrostatically tuned the electronic states from each of the two coexisting moiré superlattices and the interactions between them. When both moiré superlattices contribute equally to the electrical transport, we report a type of inter-moiré Hofstadter butterfly. Its Brown-Zak oscillation corresponds to one of the intermediate quasicrystal length scales of the reconstructed moiré-of-moiré superlattice, shedding light on emergent physics from competing atomic orders.

DOI: 10.1103/PhysRevB.110.115404

I. INTRODUCTION

When two layers of a van der Waals (vdW) material are placed on top of each other misaligned by a small twist angle, the band structure of the beating pattern (moiré superlattice) can host a high density of states (DOS) arising from near dispersionless (flat) bands. In an interacting electron context, this diverging DOS drives the system toward behavior where electron correlations and localization become dominant, leading to exotic emergent quantum phenomena distinctly different from the behavior of the original material, including superconductivity, ferromagnetism, and correlated insulator and quantum anomalous Hall states [1–10]. In twisted trilayer graphene (tTLG), where a third graphene layer is added on top of conventional twisted bilayer graphene (tBLG) [11–19], a second twist angle becomes available for additional combinations [20]. The richness of possibilities with two independent twist angles elevates tTLG to a system of uniquely different material properties: (1) when the two twist angles *alternate*, that is, are equal in magnitude but opposite in direction (twist back), the original tBLG moiré states are preserved but enhanced with higher critical temperature and electrostatic tunability [13,14,16]. (2) When the two twist angles are *consecutive* (continued twisting), the transport signature of new families of quantum states was discovered at an extremely low carrier density on the order of 10^{10} cm^{-2}, arising from a higher-order moiré-of-moiré (MoM) superlattice [12]. While case (1) is well understood in the context of moiré physics, the microscopic mechanisms for the behavior in case (2) remain elusive due to the intrinsic complexity of the underlying atomic structure. The two sets of moiré superlattices that underlie case (2) behavior interact to give rise to a plethora of emergent length scales [11,12,21,22], and both contribute and compete in determining the transport behavior. Similar atomic reconstructions have also been reported in hexagonal boron nitride (hBN)/graphene/hBN sandwiches [23–27], where a single piece of graphene is modulated by hBN, instead of more complex competition between three equally deformable graphene layers.

Here, we systematically study the interplay between the two moiré superlattices and their mutual role in determining the emergent quantum phenomena in a dual-gated consecutively twisted tTLG device. Figure 1(a) shows the schematic representation of the tTLG stack, where three pieces of monolayer graphene (MLG) flakes are sequentially picked up and transferred on top of each other, with two consecutive twist angles of 1.33 ° ± 0.03 ° (1.64 ° ± 0.04 °) between the top and middle (middle and bottom) layers. The two twist angles are chosen to be different so that the transport signature of each moiré superlattice can be isolated, corresponding to [see Fig. 1(b) schematic] a moiré superlattice constant of 10.6 nm for the top moiré (yellow) superlattice and 8.6 nm for the bottom moiré (purple) superlattice. Both twist angles are sufficiently different from the previously reported tBLG magic angle, and correlated insulator and superconducting states are not expected to emerge from any of the individual moiré superlattice.

The sample is etched into the Hall bar geometry for magnetotransport measurements [Fig. 1(b)], conducted in a ^{3}He/^{4}He dilution refrigerator at a base temperature of ∼10 mK. A global Si bottom gate (V_b) and a graphite top gate (V_t) are used

*Contact author: kewang@umn.edu

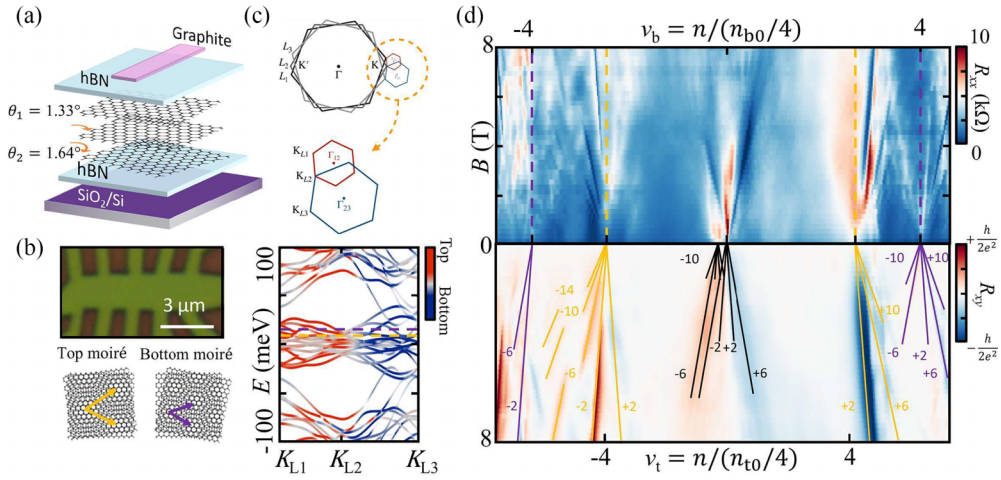

FIG. 1. Coexisting moiré superlattices in twisted trilayer graphene (tTLG). (a) Schematic image of the graphite-gated tTLG stack. (b) Upper: Optical image of the Hall bar sample. Lower: Schematic images of the top (bottom) moiré superlattice, whose lattice vectors are drawn as yellow (purple) arrows. (c) Upper: Schematic images of the Brillouin zone of the three individual MLG layers. The zoom-in image shows the two moiré mini-Brillouin zones with different sizes formed between the adjacent bilayer pairs. Lower: Calculated band structure. The red and blue colors represent the layer polarization of charge carriers. The energy levels corresponding to $\nu_t = \pm 4$ ($\nu_b = \pm 4$) are indicated by the yellow (purple) dashed lines. (d) The measured four-probe resistance R_{xx} and R_{xy} as a function of top (bottom) moiré filling factors (number of charges per moiré unit cell) and the magnetic field B. Two sets of satellite fans are observed to originate from the band-insulator states of the top (bottom) moiré superlattice, indicated by yellow (purple) lines.

for tuning the overall carrier density n in tTLG via capacitive gating with total gate potential ($V_b + \alpha V_t$, where α is the capacitive ratio between bottom and top gate). In addition, the two gates are used for tuning the relative distribution of such charge carriers among the two moiré superlattices ($V_b - \alpha V_t$) via an out-of-plane electrical field (displacement field D, positive when $V_b > \alpha V_t$). The dual-gate geometry and the addition of an out-of-plane electric field allow us to control the carrier distribution among the three layers. This enables us to enhance or suppress the contribution from each individual moiré superlattice to the transport behavior.

II. COEXISTING MOIRÉ SUPERLATTICES

Figure 1(d) shows the measured four-probe longitudinal (R_{xx}) and transverse resistance (R_{xy}) as a function of the out-of-plane magnetic field B, and moiré filling factors $\nu_t = 4n/n_{t0}(\nu_b = 4n/n_{b0})$. Here, n_{t0} (n_{b0}) corresponds to carrier density when four charge carriers occupy per unit cell of the top (bottom) moiré superlattices, denoted as $\nu_t = \pm 4$ ($\nu_b = \pm 4$), where satellite fans emerging from band-insulator states of the top (bottom) moiré superlattice are observed. At $\nu_t = \pm 4$ ($\nu_b = \pm 4$), the transport features of a Landau fan diagram are noticeably less well defined than that expected from an individual tBLG moiré superlattice [1–3] due to the presence of the additional bottom (top) graphene layer disrupting the Landau level (LL) formation in the top (bottom) moiré superlattice. The band insulator states ($\nu = \pm 4$) of each moiré superlattice also demonstrates semimetallic temperature dependence due to the third graphene layer and the absence of a gap at the edge of each set of moiré bands. A more detailed analysis on the temperature dependence of the band insulator states is discussed in Supplemental Material Sec. S4 [28] (see also Refs. [29–50] therein). The satellite Landau fan indices follow a sequence of tTLG (2, 6, 10, …) [13,14], in contrast with that from an individual tBLG moiré superlattice (4, 8, 12, …) [1–3], confirming the crucial role of the extra graphene layer in shaping the transport signature of each moiré superlattice.

The behavior of the tTLG system has unique features that are different from those of tBLG, see Fig. 1(c), where K_{L1}, K_{L2}, and K_{L3} denote the K points of the top, middle, and bottom graphene layers, respectively. Bands belonging to top and bottom moiré superlattices hybridize and compete in determining the overall transport behavior of tTLG. The red (blue) color of the bands marks the polarization (relative concentration) of charge carriers in the top (bottom) moiré superlattices, with red (blue) corresponding to carriers residing exclusively in the top (bottom) and middle graphene layers. At band insulator states of the top (bottom) moiré, denoted by a yellow (purple) dashed line, a satellite fan is observed, with its transport features compromised by the interference from the bottom (top) moiré (whose band is partially filled).

III. TUNABLE PROXIMITY EFFECT BETWEEN TWO MOIRÉ SUPERLATTICES

To confirm the above picture, we demonstrate that this interference is tunable by a displacement field D. For ease of demonstration, we first tune the device into the regime where the top moiré state dominates the transport over the bottom moiré state (in other words, charges are primarily occupying the top and middle graphene layers) and measure the satellite fan from the top moiré state, while tuning the relative contribution of the bottom moiré state with the D field.

Starting with the electron side of the top moiré fan near $\nu_t = 4$ at $D = -0.11$ V/nm, the Shubnikov–de Hass (SdH)

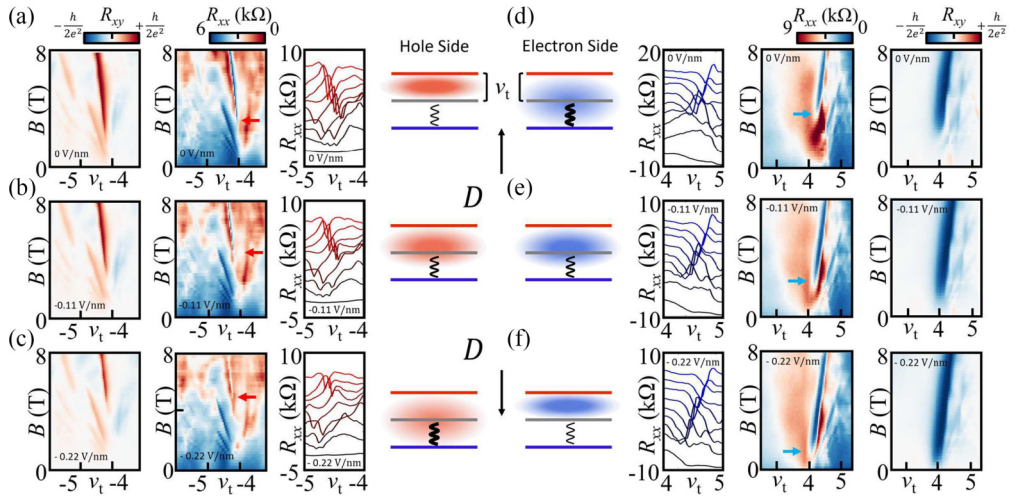

FIG. 2. Tunable proximity effect between two moiré superlattices. Measured four-probe transverse resistance R_{xy} (left), longitudinal resistance R_{xx} (middle), one-dimensional (1D) profiles of R_{xx} as a function of ν_t at different B fields (right) near the hole-type band-insulator state of the top moiré at $\nu_t = -4$, and schematics of relative charge distribution at (a) $D = 0$ V/nm, (b) $D = -0.11$ V/nm, and (c) $D = -0.22$ V/nm. 1D profiles of R_{xx} range from 0 T (black) to 8 T (red) with a 1 T increment, which are vertically offset to enhance visibility. The magnetic field at which the Shubnikov–de Hass (SdH) oscillations from the first Landau level (LL) starts to emerge increases when a more negative D field is applied, as the holes in the top moiré superlattice move toward the bottom graphene, enhancing the interference (represented by a thicker wavy line in the schematics). 1D profiles of R_{xx} as a function of ν_t at different B fields (left), longitudinal resistance R_{xx} (middle), transverse resistance R_{xy} (right) near the electron-type band-insulator state of the top moiré at $\nu_t = +4$, and schematics of relative charge distribution at (d) $D = 0$ V/nm, (e) $D = -0.11$ V/nm, and (f) $D = -0.22$ V/nm. 1D profiles of R_{xx} range from 0 T (black) to 8 T (blue) with a 1 T increment, which are vertically offset to enhance visibility. In contrast with the hole side, the magnetic field at with the SdH oscillations from the first LL starts to emerge decreases with a more negative D field, as the electrons holes in the top moiré superlattice migrates away from the bottom graphene, suppressing the interference (represented by a thinner wavy line in the schematics). In all cases, arrows show the magnetic field at which the SdH oscillations from the first LL start to emerge.

oscillation from the first LL appears at around $B = 2$ T [see Fig. 2(e)]. When the displacement field becomes more negative, at $D = -0.22$ V/nm, electrons move toward the top moiré superlattice [Fig. 2(f)]. The transport signature from the LLs in the top moiré superlattice becomes more prominent with reduced interference from the bottom layer. As a result, the SdH oscillation emerges at a lower magnetic field of $B = 0.5$ T. When the displacement field becomes more positive at $D = 0$ V/nm, electrons move closer to the bottom moiré superlattice [Fig. 2(d)], enhancing its interference, and resulting in delayed emergence of the SdH oscillation at $B = 3$ T. One-dimensional (1D) profiles of R_{xx} at different B fields, ranging from 0 T (black) to 8 T (red), quantitatively demonstrate the evolution of SdH oscillations in the top moiré superlattice, as the D field varies. The resistance dip, corresponding to when the Fermi level is in the energy gap between the first and second LLs in the top moiré superlattice, emerges at a higher B field when a more negative D field is applied. This is expected due to the enhanced interference from the bottom graphene, which leads to the broadening of LLs. As a result, a higher magnetic field is required to increase the energy separation between LLs and maintain the Fermi level within a well-defined gap.

For the hole side of the top moiré fan near $\nu_t = -4$, the dependence on D is the opposite [Figs. 2(a)–2(c)], as expected from this physics picture. As D increases (decreases), the hole type charge carrier migrates toward (away from) the top moiré superlattice, leading to a more pronounced (compromised) satellite fan diagram with the SdH oscillation starting at a lower (higher) B field.

IV. TUNABLE HIERARCHY BETWEEN TWO MOIRÉ SUPERLATTICES

To understand the competition between the two coexisting moiré superlattices, we tune the device into the regime in which transport signatures from both moiré superlattices are both present. Figures 3(a) and 3(b) show measured four-probe resistances R_{xx} and R_{xy} as functions of moiré filling factors ν_t and ν_b and perpendicular displacement fields D at $B = 4$ T (taken from another device region in Sample #1 with similar quality). A plethora of magnetotransport features belonging to LLs from five Fermi surfaces near charge neutrality point ($\nu_t, \nu_b = 0$) and four band insulator states ($\nu_t, \nu_b = \pm 4$) are observed, as the top and bottom moiré superlattices compete to dictate the transport behavior.

We now focus on the carrier density range between $\nu_t = +4$ and $\nu_b = +4$ [Figs. 3(c) and 3(d)], where electron-type LLs from the top moiré superlattice (number of LLs filled $N_t = 1, 2, \ldots$) and hole type from the bottom moiré superlattice (number of LLs filled $N_b = -1, -2, \ldots$) coexist at any given carrier density and compete in dictating the overall transport behavior. The outcome of such competition can be determined by tuning the hierarchy with D fields. For each moiré, standard SdH oscillations in R_{xx} [Fig. 3(c)] are observed with corresponding R_{xy} plateaus [Fig. 3(d)], with R_{xx}

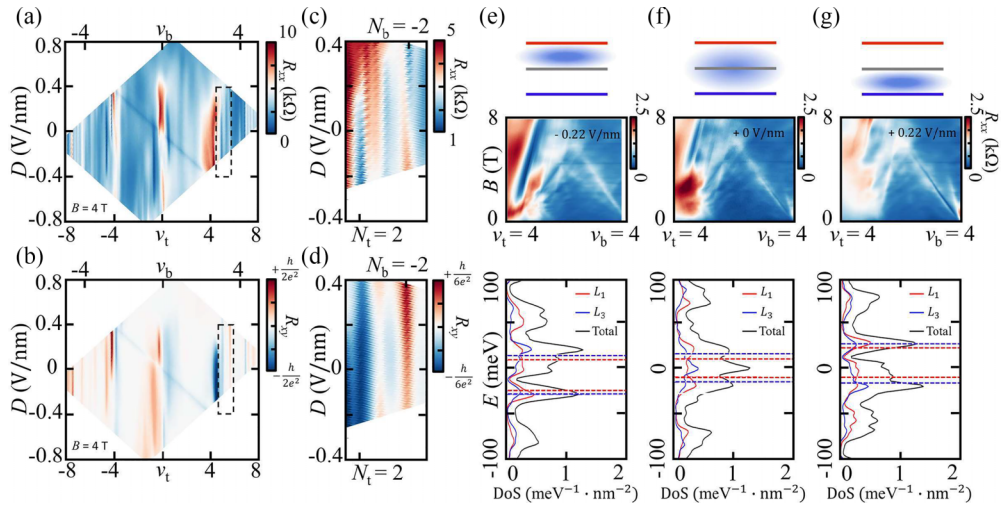

FIG. 3. Tunable hierarchy between two moiré superlattices. (a) R_{xx} and (b) R_{xy} as a function of carrier density and perpendicular displacement fields measured at $B = 4$ T. (c) and (d) zoom in on regions outlined by dashed boxes in (a) and (b), respectively. The stability of Shubnikov–de Hass (SdH) oscillations from Landau levels in the top moiré superlattice alternates with that of the bottom moiré superlattice as the D field changes. (e)–(g) The top (bottom) graphene competes for the middle layer in dominating the transport signature with that from top (bottom) moiré superlattice. The result of such competition can be tuned by displacement field (e) $D = -0.22$ V/nm, (f) $D = 0$ V/nm, and (g) $D = +0.22$ V/nm. (Top row) Schematics of electron distribution over the top (red), middle (gray), and bottom (blue) graphene layer. The electrons in the middle graphene move closer to the bottom (top) graphene as D increases (decreases), participating more in pronouncing the transport signature of the bottom (top) moiré. (Middle row) R_{xx} measured at carrier density in between $\nu_t = +4$ and $\nu_b = +4$. As D increases (decreases), the satellite fan of the winning bottom (top) moiré lattice is more visible, at the cost of the top (bottom) moiré fan being suppressed. (Bottom row) This is consistent with the calculated density of states (DOS) near $\nu_t = +4$ and $\nu_b = +4$, where a decreasing (increasing) trend in DOS per top (bottom) graphene layer L_1 (L_3) is found as the D field becomes more positive. The red, blue, and black curves correspond to the DOS in the top and bottom graphene layers and in the entire twisted trilayer graphene (tTLG), respectively. The red (blue) dashed lines indicate the energies corresponding to ν_t (ν_b) $= \pm 4$.

dips and R_{xy} quantization more (less) well defined from the dominant (dominated) moiré superlattice. When the D field becomes more positive (negative), electrons distribute toward the bottom (top) moiré superlattice, allowing it to dominate the transport signature more. As a result, at a positive D field, the R_{xx} resistance dips and R_{xy} plateaus at $N_b = -2$, corresponding to the dominant moiré being more well defined and quantized at the price of transport signatures from $N_t = 2$ of the dominated moiré becoming weaker, with a higher R_{xx} dip resistance and a R_{xy} resistance deviating from the expected quantization. The reverse is observed at a negative D field, when the balance of the competition is flipped.

The same physics can also be confirmed by observing the evolution of satellite fans from both moiré superlattices at the intermediate carrier density range between $\nu_t = +4$ and $\nu_b = +4$ at different D fields. When a positive D field is applied [Fig. 3(g)], the electrons move toward the bottom moiré superlattice, whose fan becomes more prominent than the feature from the top moiré superlattice. In contrast, when a negative D field is applied, the electrons move toward the top moiré superlattice, whose fan is now more visible at the cost of a smeared-out bottom moiré fan [Fig. 3(e)]. This is consistent with the calculated DOS near $\nu_t = +4$ and $\nu_b = +4$, where a decreasing (increasing) trend in DOS per top (bottom) graphene layer L_1 (L_3) is found as the D field becomes more positive [bottom row of Figs. 3(e)–3(g)]. At $D = 0$ V/nm [Fig. 3(f)], the device is tuned into the strong-coupling regime, where both moiré patterns contribute equally and therefore compete in determining the transport signature.

V. INTER-MOIRÉ HOFSTADTER BUTTERFLY

Figure 4(a) shows a zoom-in high-resolution scan of the measured four-probe conductance, where a complex emergent pattern is observed, which we refer to as a type of *inter-moiré Hofstadter butterfly*. Longitudinal conductance peaks are observed at $B = 7.4, 4.9, 3.7, 3.0, 2.5, 2.1$ T, …, shown as horizontal lines (dashed) in four-probe resistance [Fig. 4(a)]. The inset shows σ_{xx} as a function of B, averaged over the entire carrier density range of the color plot, signifying the magnetic field at which local conductance maxima are found along horizontal lines in the color plot (marked by arrows in inset and dashed lines in color plots), or Brown-Zak oscillations [51,52]. These magnetic field values correspond to $1/n$ (where $n = 2, 3, 4, 5, 6, 7, \ldots$) flux quanta ($\phi_0$) for a unit cell size of 283 ± 7 nm^2 (or lattice constant of 18.1 ± 0.2 nm).

In addition, a high-order conductance peak is observed at a magnetic field corresponding to 2 flux quanta per 5 of such unit cells [51]. This corresponds to a second-order Brown-Zak oscillation ($2/n$ flux quanta), like that observed in the conventional Hofstadter butterfly with state-of-the-art device quality [51–54]. The presence of the second-order feature in the Brown-Zak oscillation indicates the stability and homogeneity of the reconstructed higher-order lattice length scale of ∼18 nm.

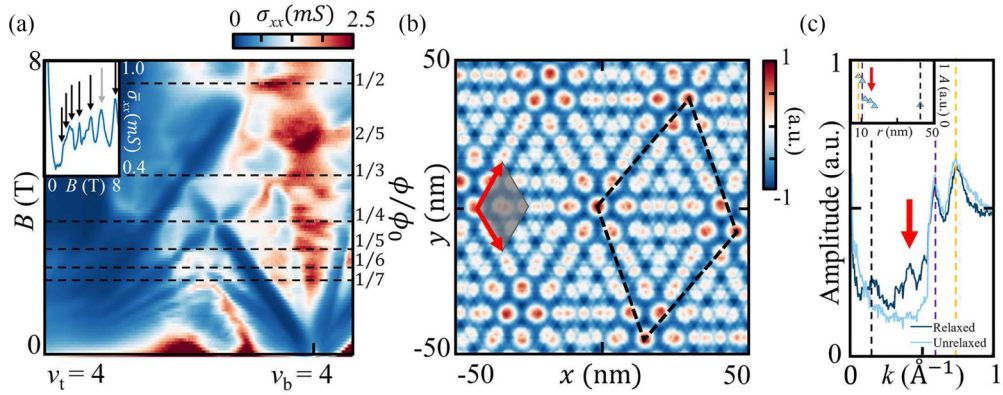

FIG. 4. Inter-moiré Hofstadter butterfly. (a) Conductance σ_{xx} as a function of filling factors and the magnetic field (left axis) or magnetic flux $\phi = BS$ in the unit of flux quantum ϕ_0 (right axis). Sequence of $\phi/\phi_0 = 1/n$ is outlined by black dashed lines. Insert: σxx as a function of B, averaged over the entire carrier density range of the color plot, signifying the magnetic field at which conductance peaks are found along horizontal lines in the color plot (marked by arrows in inset and dashed lines in color plots). (b) Simulation of relaxed atomic landscape of twisted trilayer graphene (tTLG), with the color scale plotting relaxed total misfit energy landscape. The periodicity of the inter-moiré Brown-Zak oscillation (in $1/B$) corresponds to a unit cell (gray shade) size 283 ± 7 nm^2, or lattice (red arrows) constant of 18.1 ± 0.2 nm. (c) The length scale agrees with one of the most prominent among a plethora of coexisting length scales in tTLG, shown by calculated Fourier spectrum of relaxed tTLG. Peaks are found at dominant length scales at lattice constant of moiré-of-moiré (MoM) superlattice (black dashed, 42.8 nm), top moiré superlattice (orange dashed, 10.5 nm), bottom moiré superlattice (blue dashed, 8.4 nm), and additionally at intermediate length scale between 15 and 20 nm (arrow) responsible for the observed Brown-Zak oscillation. Inset: Dominate length scales and their relative weight.

The previously reported Hofstadter butterfly in hBN-graphene or tBLG [55–58] is observed when fans from the satellite peak and the Dirac peak overlap, whose periodicity in $1/B$ is a consequence of emergent moiré periodicity. In contrast, the inter-moiré Hofstadter butterfly results from two sets of satellite fans crossing over (without participation of the main fan from charge neutrality point), each belonging to a superlattice with distinct lattice constant. The inter-moiré butterfly is therefore a signature of higher-order superlattice periodicity reconstructed from two coexisting moiré superlattices. The unit cell size of 283 ± 7 nm^2 extracted from the inter-moiré butterfly agrees with one of the intermediate length scales in the relaxed atomic landscape of tTLG [shaded rhombus in Fig. 4(b), with lattice vectors labeled by red arrows], one that is most prominent among a plethora of length scales that coexist in consecutive tTLG [Fig. 4(c)] [20]. The relaxed atomic landscape of tTLG is obtained based on a continuum relaxation model in local configuration space [44] by minimizing the total energy with respect to the relaxation displacement vector. The details of the model are elaborated in Supplemental Material Sec. S9 [28] (see also Refs. [29–50] therein). Notably, the MoM superlattice has a unit cell size ($\sim$1527 nm^2) that is $\sim$5.4 times larger, with a corresponding Brown-Zak oscillation expected at magnetic field values of $B = 2.70, 1.34, 0.90, 0.67, 0.54, 0.46$ T, …, before SdH oscillations of the two competing fan diagram start to emerge.

It is worth noting that the Brillouin zone (BZ) oscillations observed in our device correspond to higher-order MoM length scales only, in contrast with the previously reported doubly aligned hBN/graphene/hBN structure in which BZ oscillations from each moiré superlattice are also visible [23]. This is consistent with the observation of tunable competing moiré electronic states in tTLG (Figs. 2 and 3), where the electronic signatures from both moiré patterns are compromised by each other, and the reconstructed length scale dictates the transport behavior. In doubly aligned hBN/graphene/hBN, all electrons reside in a single atomic layer of graphene. The moiré states from lattice modulation by each aligned hBN coexist but do not compete to comprise each other or yield higher-order atomic reconstruction.

Our observation of an inter-moiré butterfly provides experimental evidence for atomic lattice reconstruction in tTLG. In tBLG, the lattice reconstruction effects are a monotonous function of the twist angle. Lattice reconstruction is weak above a critical twist angle of $\sim 1^\circ$. In contrast, in tTLG, the strength of lattice reconstruction in tTLG sensitively depends on the difference between the twist angles as well as the moiré harmonics, in addition to the absolute values of the twist angles. Theoretical predictions of the real-space relaxed pattern [44,59] or local DOS maps [60] in tTLG show that a dominating MoM pattern can appear at twist angles $>1^\circ$. Our experimental observation indicates that tTLG at such a twist angle combination (1.33° and 1.64°) indeed experiences a significant amount of lattice reconstruction, with the BZ oscillations corresponding to higher-order length scale ($\sim$18 nm) instead of any of the moiré length scales (10.6 and 8.6 nm). The observed lattice construction may be particularly relevant in realizing predicted quantum phases in tTLG that are sensitive to the microscopic landscape of the lattice reconstruction in tTLG, such as correlated and topological phases in magic-angle helical trilayer graphene [21].

VI. SUMMARY

In conclusion, we measured magnetotransport in a consecutively tTLG device, with twist angles of $1.33^\circ \pm 0.03^\circ$ and $1.64^\circ \pm 0.04^\circ$. We observed two sets of satellite Landau

fans, each belonging to one of two coexisting moiré superlattices. The two moiré superlattices compete in determining the transport signature of the tTLG at carrier density on the order of $10^{12}\,\mathrm{cm}^{-2}$, or typical moiré filling. We show that the strength and the hierarchy of the inter-moiré interaction can be tuned electrostatically, confirming the underlying physics picture. When the transport signatures of two moiré superlattices are equally present, we observe a type of inter-moiré Hofstadter butterfly, the periodical pattern of which agrees with a higher-order quasilattice reconstructed from the two moiré superlattices. In this paper, we provide a comprehensive understanding of the complex interaction between coexisting atomic orders in tTLG and how higher-order periodicities and their transport signatures emerge from such competition. This opens a door toward understanding the intriguing microscopic mechanisms of emergent quantum phenomena in twisted multilayer 2D material platforms.

ACKNOWLEDGMENT

We thank A. Chubukov, B. Shklovski, and Y. Huang for helpful discussion. This paper was supported by National Science Foundation (NSF) DMREF Awards No. DMR-1922165 and No. DMR-1922172, ARO MURI Grant No. W911NF-14-1-0247, and Simons Foundation Award No. 896626. Nanofabrication was conducted in the Minnesota Nano Center, which is supported by the NSF through the National Nano Coordinated Infrastructure Network, Award No. NNCI-1542202. Z.Z. is supported by a Stanford Science fellowship. Portions of the hexagonal boron nitride material used in this paper were provided by K.W. and T.T. K.W. and T.T. acknowledge support from the JSPS KAKENHI (Grants No. 20H00354, No. 21H05233, and No. 23H02052) and World Premier International Research Center Initiative, MEXT, Japan.

[1] Y. Cao, V. Fatemi, S. Fang, K. Watanabe, T. Taniguchi, E. Kaxiras, and P. Jarillo-Herrero, Unconventional superconductivity in magic-angle graphene superlattices, Nature (London) **556**, 43 (2018).

[2] Y. Cao, V. Fatemi, A. Demir, S. Fang, S. L. Tomarken, J. Y. Luo, J. D. Sanchez-Yamagishi, K. Watanabe, T. Taniguchi, E. Kaxiras *et al.*, Correlated insulator behaviour at half-filling in magic-angle graphene superlattices, Nature (London) **556**, 80 (2018).

[3] M. Yankowitz, S. Chen, H. Polshyn, Y. Zhang, K. Watanabe, T. Taniguchi, D. Graf, A. F. Young, and C. R. Dean, Tuning superconductivity in twisted bilayer graphene, Science **363**, 1059 (2019).

[4] X. Lu, P. Stepanov, W. Yang, M. Xie, M. A. Aamir, I. Das, C. Urgell, K. Watanabe, T. Taniguchi, G. Zhang *et al.*, Superconductors, orbital magnets and correlated states in magic-angle bilayer graphene, Nature (London) **574**, 653 (2019).

[5] A. L. Sharpe, E. J. Fox, A. W. Barnard, J. Finney, K. Watanabe, T. Taniguchi, M. A. Kastner, and D. Goldhaber-Gordon, Emergent ferromagnetism near three-quarters filling in twisted bilayer graphene, Science **365**, 605 (2019).

[6] K. P. Nuckolls, M. Oh, D. Wong, B. Lian, K. Watanabe, T. Taniguchi, B. A. Bernevig, and A. Yazdani, Strongly correlated Chern insulators in magic-angle twisted bilayer graphene, Nature (London) **588**, 610 (2020).

[7] I. Das, X. Lu, J. Herzog-Arbeitman, Z.-D. Song, K. Watanabe, T. Taniguchi, B. A. Bernevig, and D. K. Efetov, Symmetry-broken Chern insulators and Rashba-like Landau-level crossings in magic-angle bilayer graphene, Nat. Phys. **17**, 710 (2021).

[8] Y. Saito, J. Ge, L. Rademaker, K. Watanabe, T. Taniguchi, D. A. Abanin, and A. F. Young, Hofstadter subband ferromagnetism and symmetry-broken Chern insulators in twisted bilayer graphene, Nat. Phys. **17**, 478 (2021).

[9] S. Wu, Z. Zhang, K. Watanabe, T. Taniguchi, and E. Y. Andrei, Chern insulators, Van Hove singularities and topological flat bands in magic-angle twisted bilayer graphene, Nat. Mater. **20**, 488 (2021).

[10] D. Waters, E. Thompson, E. Arreguin-Martinez, M. Fujimoto, Y. Ren, K. Watanabe, T. Taniguchi, T. Cao, D. Xiao, and M. Yankowitz, Mixed-dimensional moiré systems of twisted graphitic thin films, Nature (London) **620**, 750 (2023).

[11] A. Uri, S. C. de la Barrera, M. T. Randeria, D. Rodan-Legrain, T. Devakul, P. J. D. Crowley, N. Paul, K. Watanabe, T. Taniguchi, R. Lifshitz *et al.*, Superconductivity and strong interactions in a tunable moiré quasicrystal, Nature (London) **620**, 762 (2023).

[12] X. Zhang, K.-T. Tsai, Z. Zhu, W. Ren, Y. Luo, S. Carr, M. Luskin, E. Kaxiras, and K. Wang, Correlated insulating states and transport signature of superconductivity in twisted trilayer graphene superlattices, Phys. Rev. Lett. **127**, 166802 (2021).

[13] J. M. Park, Y. Cao, K. Watanabe, T. Taniguchi, and P. Jarillo-Herrero, Tunable strongly coupled superconductivity in magic-angle twisted trilayer graphene, Nature (London) **590**, 249 (2021).

[14] Z. Hao, A. M. Zimmerman, P. Ledwith, E. Khalaf, D. H. Najafabadi, K. Watanabe, T. Taniguchi, A. Vishwanath, and P. Kim, Electric field–tunable superconductivity in alternating-twist magic-angle trilayer graphene, Science **371**, 1133 (2021).

[15] Z. Ma, S. Li, Y.-W. Zheng, M.-M. Xiao, H. Jiang, J.-H. Gao, and X. C. Xie, Topological flat bands in twisted trilayer graphene, Science Bulletin **66**, 18 (2021).

[16] X. Liu, N. J. Zhang, K. Watanabe, T. Taniguchi, and J. I. A. Li, Isospin order in superconducting magic-angle twisted trilayer graphene, Nat. Phys. **18**, 522 (2022).

[17] S. Turkel, J. Swann, Z. Zhu, M. Christos, K. Watanabe, T. Taniguchi, S. Sachdev, M. S. Scheurer, E. Kaxiras, C. R. Dean *et al.*, Orderly disorder in magic-angle twisted trilayer graphene, Science **376**, 193 (2022).

[18] H. Kim, Y. Choi, C. Lewandowski, A. Thomson, Y. Zhang, R. Polski, K. Watanabe, T. Taniguchi, J. Alicea, and S. Nadj-Perge, Evidence for unconventional superconductivity in twisted trilayer graphene, Nature (London) **606**, 494 (2022).

[19] D. Park, C. Park, E. Ko, K. Yananose, R. Engelke, X. Zhang, K. Davydov, M. Green, S. H. Park, J. H. Lee *et al.*, Tunable

incommensurability and spontaneous symmetry breaking in the reconstructed moiré-of-moiré lattices, arXiv:2402.15760.

[20] Z. Zhu, S. Carr, D. Massatt, M. Luskin, and E. Kaxiras, Twisted trilayer graphene: A precisely tunable platform for correlated electrons, Phys. Rev. Lett. **125**, 116404 (2020).

[21] T. Devakul, P. J. Ledwith, L.-Q. Xia, A. Uri, S. C. de la Barrera, P. Jarillo-Herrero, and L. Fu, Magic-angle helical trilayer graphene, Sci. Adv. **9**, eadi6063 (2023).

[22] L.-Q. Xia, S. C. de la Barrera, A. Uri, A. Sharpe, Y. H. Kwan, Z. Zhu, K. Watanabe, T. Taniguchi, D. Goldhaber-Gordon, L. Fu *et al.*, Helical trilayer graphene: A moiré platform for strongly-interacting topological bands, arXiv:2310.12204.

[23] Z. Wang, Y. B. Wang, J. Yin, E. Tóvári, Y. Yang, L. Lin, M. Holwill, J. Birkbeck, D. J. Perello, S. Xu *et al.*, Composite super-moiré lattices in double-aligned graphene heterostructures, Sci. Adv. **5**, eaay8897 (2019).

[24] L. Wang, S. Zihlmann, M.-H. Liu, P. Makk, K. Watanabe, T. Taniguchi, A. Baumgartner, and C. Schönenberger, New generation of moiré superlattices in doubly aligned hBN/Graphene/hBN heterostructures, Nano Lett. **19**, 2371 (2019).

[25] M. Anđelković, S. P. Milovanović, L. Covaci, and F. M. Peeters, Double moiré with a twist: Supermoiré in encapsulated graphene, Nano Lett. **20**, 979 (2020).

[26] J. Hu, J. Tan, M. M. Al Ezzi, U. Chattopadhyay, J. Gou, Y. Zheng, Z. Wang, J. Chen, R. Thottathil, J. Luo *et al.*, Controlled alignment of supermoiré lattice in double-aligned graphene heterostructures, Nat. Commun. **14**, 4142 (2023).

[27] M. K. Jat, P. Tiwari, R. Bajaj, I. Shitut, S. Mandal, K. Watanabe, T. Taniguchi, H. R. Krishnamurthy, M. Jain, and A. Bid, Higher order gaps in the renormalized band structure of doubly aligned hBN/Bilayer graphene moiré superlattice, Nat. Commun. **15**, 2335 (2024).

[28] See Supplemental Material at http://link.aps.org/supplemental/10.1103/PhysRevB.110.115404 for a more detailed analysis on the temperature dependence of the band insulator states; details of sample preparation and device fabrication; transport signature in other device regions and samples; detailed transport signature of the moiré band-insulator states; defination of the zero perpendicular displacement field; evolution of density of states in each moiré superlattice under displacement fields; extracting the unit cell size from the inter-moiré butterfly; details of band structure calculation; and details of relaxed total energy landscape calculation, which includes Refs. [29–50].

[29] Y. Saito, J. Ge, K. Watanabe, T. Taniguchi, and A. F. Young, Independent superconductors and correlated insulators in twisted bilayer graphene, Nat. Phys. **16**, 926 (2020).

[30] A. K. Geim, Graphene: Status and prospects, Science **324**, 1530 (2009).

[31] C. R. Dean, A. F. Young, I. Meric, C. Lee, L. Wang, S. Sorgenfrei, K. Watanabe, T. Taniguchi, P. Kim, and K. L. Shepard, Boron nitride substrates for high-quality graphene electronics, Nat. Nanotechnol. **5**, 722 (2010).

[32] L. Wang, I. Meric, P. Y. Huang, Q. Gao, Y. Gao, H. Tran, T. Taniguchi, K. Watanabe, L. M. Campos, and D. A. Muller, One-dimensional electrical contact to a two-dimensional material, Science **342**, 614 (2013).

[33] X. Lin, C. Li, K. Su, and J. Ni, Energetic stability and spatial inhomogeneity in the local electronic structure of relaxed twisted trilayer graphene, Phys. Rev. B **106**, 075423 (2022).

[34] B. Padhi, A. Tiwari, T. Neupert, and S. Ryu, Transport across twist angle domains in moiré graphene, Phys. Rev. Res. **2**, 033458 (2020).

[35] Y.-H. Zhang, H. C. Po, and T. Senthil, Landau level degeneracy in twisted bilayer graphene: Role of symmetry breaking, Phys. Rev. B **100**, 125104 (2019).

[36] K. Hejazi, C. Liu, and L. Balents, Landau levels in twisted bilayer graphene and semiclassical orbits, Phys. Rev. B **100**, 035115 (2019).

[37] S. Yuan, R. Roldán, and M. I. Katsnelson, Landau level spectrum of ABA- and ABC-Stacked trilayer graphene, Phys. Rev. B **84**, 125455 (2011).

[38] T. Taychatanapat, K. Watanabe, T. Taniguchi, and P. Jarillo-Herrero, Quantum Hall effect and Landau-level crossing of Dirac fermions in trilayer graphene, Nat. Phys. **7**, 621 (2011).

[39] R. Bistritzer and A. H. MacDonald, Moiré bands in twisted double-layer graphene, Proc. Natl. Acad. Sci. USA **108**, 12233 (2011).

[40] J. H. Gosling, O. Makarovsky, F. Wang, N. D. Cottam, M. T. Greenaway, A. Patanè, R. D. Wildman, C. J. Tuck, L. Turyanska, and T. M. Fromhold, Universal mobility characteristics of graphene originating from charge scattering by ionised impurities, Commun. Phys. **4**, 30 (2021).

[41] G. M. Rutter, S. Jung, N. N. Klimov, D. B. Newell, N. B. Zhitenev, and J. A. Stroscio, Microscopic polarization in bilayer graphene, Nat. Phys. **7**, 649 (2011).

[42] S. Kim, D. Kim, K. Watanabe, T. Taniguchi, J. H. Smet, and Y. Kim, Orbitally controlled quantum Hall states in decoupled two-bilayer graphene sheets, Adv. Sci. **10**, 2300574 (2023).

[43] S. Fang and E. Kaxiras, Electronic structure theory of weakly interacting bilayers, Phys. Rev. B **93**, 235153 (2016).

[44] Z. Zhu, P. Cazeaux, M. Luskin, and E. Kaxiras, Modeling mechanical relaxation in incommensurate trilayer van der Waals heterostructures, Phys. Rev. B **101**, 224107 (2020).

[45] P. Cazeaux, M. Luskin, and D. Massatt, Energy minimization of two dimensional incommensurate heterostructures, Arch. Rational Mech. Anal. **235**, 1289 (2020).

[46] E. Kaxiras and M. S. Duesbery, Free energies of generalized stacking faults in Si and implications for the brittle-ductile transition, Phys. Rev. Lett. **70**, 3752 (1993).

[47] S. Carr, D. Massatt, S. B. Torrisi, P. Cazeaux, M. Luskin, and E. Kaxiras, Relaxation and domain formation in incommensurate two-dimensional heterostructures, Phys. Rev. B **98**, 224102 (2018).

[48] S. Zhou, J. Han, S. Dai, J. Sun, and D. J. Srolovitz, van der Waals bilayer energetics: Generalized stacking-fault energy of graphene, boron nitride, and graphene/boron nitride bilayers, Phys. Rev. B **92**, 155438 (2015).

[49] G. Kresse and J. Hafner, *Ab initio* molecular dynamics for liquid metals, Phys. Rev. B **47**, 558 (1993).

[50] G. Kresse and J. Furthmüller, Efficient iterative schemes for *ab initio* total-energy calculations using a plane-wave basis set, Phys. Rev. B **54**, 11169 (1996).

[51] R. Kumar, A. Mishchenko, X. Chen, S. Pezzini, G. Auton, L. Ponomarenko, U. Zeitler, L. Eaves, V. Fal'ko, and A. Geim, High-order fractal states in graphene superlattices, Proc. Natl. Acad. Sci. USA **115**, 5135 (2018).

[52] R. Huber, M.-N. Steffen, M. Drienovsky, A. Sandner, K. Watanabe, T. Taniguchi, D. Pfannkuche, D. Weiss, and J. Eroms, Band conductivity oscillations in a gate-tunable graphene superlattice, Nat. Commun. **13**, 2856 (2022).

[53] J. Barrier, P. Kumaravadivel, R. K. Kumar, L. A. Ponomarenko, N. Xin, M. Holwill, C. Mullan, M. Kim, R. V. Gorbachev, M. D. Thompson *et al.*, Long-range ballistic transport of Brown-Zak fermions in graphene superlattices, Nat. Commun. **11**, 5756 (2020).

[54] W. Shi, S. Kahn, N. Leconte, T. Taniguchi, K. Watanabe, M. Crommie, J. Jung, and A. Zettl, High-order fractal quantum oscillations in graphene/BN superlattices in the extreme doping limit, Phys. Rev. Lett. **130**, 186204 (2023).

[55] C.-H. Park, L. Yang, Y.-W. Son, M. L. Cohen, and S. G. Louie, New generation of massless Dirac fermions in graphene under external periodic potentials, Phys. Rev. Lett. **101**, 126804 (2008).

[56] B. Hunt, J. D. Sanchez-Yamagishi, A. F. Young, M. Yankowitz, B. J. LeRoy, K. Watanabe, T. Taniguchi, P. Moon, M. Koshino, P. Jarillo-Herrero *et al.*, Massive Dirac fermions and Hofstadter butterfly in a van der Waals heterostructure, Science **340**, 1427 (2013).

[57] C. R. Dean, L. Wang, P. Maher, C. Forsythe, F. Ghahari, Y. Gao, J. Katoch, M. Ishigami, P. Moon, M. Koshino *et al.*, Hofstadter's butterfly and the fractal quantum Hall effect in moiré superlattices, Nature (London) **497**, 598 (2013).

[58] X. Lu, B. Lian, G. Chaudhary, B. A. Piot, G. Romagnoli, K. Watanabe, T. Taniguchi, M. Poggio, A. H. MacDonald, B. A. Bernevig *et al.*, Multiple flat bands and topological Hofstadter butterfly in twisted bilayer graphene close to the second magic angle, Proc. Natl. Acad. Sci. USA **118**, e2100006118 (2021).

[59] N. Nakatsuji, T. Kawakami, and M. Koshino, Multiscale lattice relaxation in general twisted trilayer graphenes, Phys. Rev. X **13**, 041007 (2023).

[60] H. Meng, Z. Zhan, and S. Yuan, Commensurate and incommensurate double moiré interference in twisted trilayer graphene, Phys. Rev. B **107**, 035109 (2023).